Gas-Phase Metal Ion Ligation: Collision-Induced Dissociation of $Fe(N_2)_x^+$ ($x = 1-5$) and $Fe(CH_2O)_x^+$ ($x = 1-4$)

Brenda L. Tjelta and P. B. Armentrout*

Department of Chemistry, University of Utah, Salt Lake City, Utah 84112

Received: August 20, 1996; In Final Form: January 14, 1997[⊗]

Thresholds for collision-induced dissociation of $Fe(N_2)_x^+$ ($x = 1-5$) and $Fe(CH_2O)_x^+$ ($x = 1-4$) with xenon are measured by using guided ion beam mass spectrometry. Values for the 0 K $(N_2)_{x-1}Fe^+-N_2$ bond energies (in eV) are determined to be 0.56 ± 0.06, 0.86 ± 0.09, 0.47 ± 0.06, 0.56 ± 0.04, and 0.64 ± 0.04 for $x = 1-5$, respectively. Values for the 0 K $(CH_2O)_{x-1}Fe^+-CH_2O$ bond energies (in eV) are determined to be 1.43 ± 0.07, 1.79 ± 0.08, 1.06 ± 0.05, and 0.83 ± 0.06 for $x = 1-4$, respectively. The bond energy for Fe^+-Xe is determined as 0.47 ± 0.08 eV. The results for the singly ligated species are in good agreement with values in the literature. These bond energies are compared with those for several other FeL_x+ series including previously published values for $Fe(CO)_x^+$ ($x = 1-5$), which are reevaluated in light of theoretical information. The observation that the relative bond strengths vary nonmonotonically with the number of ligands is discussed in terms of spin conservation and ligand field theory.

Introduction

The nature of the solvation process has been the subject of considerable study for many years.[1] One approach to obtaining a quantitative characterization of solvation has been the study of ion−solvent clusters in the gas phase. A related phenomenon is the variation in the physical and chemical properties of a metal center as the degree of ligation is varied. An important element in characterizing both solvation and ligation effects is the bond dissociation energy (BDE) of individual $(L)_{x-1}M-L$ bonds. Such thermochemical studies are of interest because they help build a database of BDEs for coordinatively unsaturated ML_x species and they provide a benchmark against which theoretical models of bonding in these compounds can be tested. Further, these studies can provide general insight into how and why thermochemistry changes with variations in ligation.

The BDEs for $Fe(H_2O)_x^+$, $Fe(CO)_x^+$, and $Fe(H_2)_x^+$ clusters have been thoroughly investigated both experimentally[2−4] and theoretically.[5−7] In this study, we extend our work on iron ligation to include dinitrogen (formally isoelectronic with CO) and formaldehyde (a polar molecule like H_2O). Bond energies for the monoligated species in both cases have been reported in the literature. Schwarz and co-workers[8] theoretically characterized the Fe^+-N_2 complex in terms of electronic structure and binding energy. Gas-phase ligand exchange reactions accompanied the theoretical study in order to experimentally "bracket" the Fe^+-N_2 BDE. Similarly, Schwarz and co-workers have estimated the Fe^+-CH_2O bond energy from relative values using $D_0[Fe^+-C_2H_4]$ as an anchor point.[9] To our knowledge, no further information, either experimental or theoretical, is available on isolated iron dinitrogen or formaldehyde complexes.

With our guided ion beam apparatus, we are able to make *direct* measurements of the Fe^+-N_2 and Fe^+-CH_2O bond energies. The present study was undertaken to obtain a self-consistent set of BDEs for $Fe(N_2)_x^+$ ($x = 1-5$) and $Fe(CH_2O)_x^+$ ($x = 1-4$) and to understand the nonmonotonic variation in the sequential bond energies. Comparison of the $Fe(N_2)_x^+$ results with those for $Fe(CO)_x^+$ allows for a comparison of isoelectronic strong and weak field ligands, while the CH_2O ligand is related to CO but much more polar. We also take this opportunity to reexamine our previously determined $(CO)_{x-1}Fe^+-CO$ BDEs[3] in light of theoretical values reported by Bauschlicher and co-workers.[6] Specifically, we investigate whether the differences between experimental and theoretical BDEs can be resolved with use of more accurate vibrational frequencies and a better estimation of the lifetime effects in our data analysis.

Experimental Section

The guided ion beam instrument on which these experiments were performed has been described in detail previously.[10,11] Ions are created in a flow tube source as described below, extracted from the source, accelerated, and passed through a magnetic sector for mass analysis. The mass-selected ions are decelerated to the desired kinetic energy and focused into an octopole beam guide. This device uses radio-frequency electric fields to trap the ions in the radial direction to ensure complete collection of reactant and product ions.[12] The octopole passes through a gas cell that contains the neutral collision partner at relatively low pressures (~0.05−0.2 mTorr). After exiting the gas cell, the unreacted parent and product ions drift to the end of the octopole, from which they are extracted, passed through a quadrupole mass filter for mass analysis, and detected with a secondary electron scintillation ion detector using standard pulse-counting techniques. Raw ion intensities are converted to cross sections as described previously.[10] We estimate absolute cross sections to be accurate to ±20%.

Laboratory (lab) energies are converted to energies in the center of mass (CM) frame using $E_{CM} = E_{lab}M/(M + m)$, where m and M are the ion and neutral masses, respectively. The absolute energy scale and corresponding full width at half-maximum (fwhm) of the ion beam kinetic energy distribution are determined by using the octopole as a retarding energy analyzer as described previously.[10] The absolute uncertainty in the energy scale is ±0.05 eV (lab). The ion energy distributions are nearly Gaussian and have a typical fwhm of 0.25−0.55 eV (lab).

Ion Source. The metal−ligand ions are formed in a 1 m long flow tube[11] operating at a pressure of 0.4−0.7 Torr with a helium flow rate of 4000−9000 standard cm^3/min. Fe^+ is produced by argon ion sputtering of an iron cathode in a flow

[⊗] Abstract published in *Advance ACS Abstracts,* February 15, 1997.

S1089-5639(96)02562-5 CCC: $14.00

of 5−10% argon in helium. $Fe(N_2)_x^+$ and $Fe(CH_2O)_x^+$ ions are formed by three-body associative reactions of Fe^+ with the ligand molecules. To form $Fe(N_2)_x^+$, nitrogen gas is added 50 cm downstream from the dc discharge. For the smaller ions, the amount of N_2 added to the flow was less than 10% of the total flow, and for the larger ones, the amount added was as much as 24% of the total flow. To introduce formaldehyde into the flow tube, paraformaldehyde is packed in copper tubing wrapped with heating tape. The sample is heated and a small flow of helium was passed over the sample to carry gaseous $(CH_2O)_x$ fragments into the flow tube. This ligand is introduced 10 cm downstream from the dc discharge.

The flow conditions used in the flow tube ion source provide approximately 10^5 collisions between an ion and the buffer gas, which should thermalize the ions both rotationally and vibrationally. We assume that the internal energy of the ions produced in this source is well described by a Maxwell−Boltzmann distribution of rotational and vibrational states corresponding to 298 K. Previous work from this laboratory has shown that this assumption is valid.[3,13−15]

The larger cluster ion beams ($x = 4$, 5) were less intense than those of the smaller ions by over an order of magnitude, as can be inferred from the relative signal to noise for the different experimental results. Presumably, these larger ions were more difficult to make because of the additional collisions in the flow tube needed for their formation. In the case of $Fe(N_2)_x^+$ ions, addition of too much N_2 to the flow tube can cause formation of nitrogen clusters, $(N_2)_{x+2}^+$, with possibly the same mass as the $Fe(N_2)_x^+$ ions. Such contamination can be ascertained by looking for the formation of N_2^+ in the mass spectra at high collision energies (up to 50 eV lab energy). The present data were collected only when evidence for such contamination was not present.

Thermochemical Analysis. As previously reported for the collision-induced (CID) cross sections of $Fe(CO)_x^+$ ($x = 3−5$)[3] and cluster ions,[16] the cross sections for CID of the more highly ligated ions examined here show a marked dependence on the Xe pressure in the gas cell due to the increasing probability of secondary collisions with increasing pressure. This pressure effect is eliminated, following a procedure developed previously,[3,17] by linearly extrapolating the cross sections to zero pressure, rigorously single-collision conditions. All cross sections shown below and all threshold analyses reported here for these species are performed on data that have been thus extrapolated. For $x = 1$ and 2, this procedure is unnecessary because no pressure dependence is observed over the Xe pressure range used (up to 0.2 mTorr).

Theory and experiment[18] have shown that endothermic cross sections can be modeled in the threshold region with eq 1,

$$\sigma(E) = \sigma_0 \sum g_i (E + E_{rot} + E_i - E_0)^n / E \qquad (1)$$

where σ_0 is an energy independent scaling factor, E is the relative translational energy of the reactants, E_{rot} is the average rotational energy of the reactants ($E_{rot} = 0.026$ eV for linear molecules and 0.039 eV for nonlinear molecules), E_0 is the reaction threshold at 0 K, and n is an adjustable parameter. The summation is over the vibrational states i having energies E_i and populations g_i, where $\sum g_i = 1$. We assume that the relative reactivity, as reflected by σ_0 and n, is the same for all vibrational states. Details about our implementation of this equation are given elsewhere.[3] Briefly, the Beyer−Swinehart algorithm[19] is used to evaluate the density of the ion vibrational states, and then the relative populations, g_i, are calculated by the appropriate Maxwell−Boltzmann distribution at 298 K.

TABLE 1: Vibrational Frequencies and Average Vibrational Energies at 298 K

species	E_{vib},[a] eV	frequency(degeneracies),[b] cm^{-1}
free N_2		2358
$Fe(N_2)^+$	0.04(0.01)	free N_2, 239(2), 318
$Fe(N_2)_2^+$	0.12(0.02)	free N_2(2), 61(2), 217(2), 261, 300, 441(2)
$Fe(N_2)_3^+$	0.19(0.02)	free N_2(3), 46(2), 53, 191(2), 207, 220, 230(2), 266(2), 279
$Fe(N_2)_4^+$ [c]	0.28(0.03)	free N_2(4), 41(2), 55(3), 194(3), 206, 228(3), 263(2), 283(3)
$Fe(N_2)_5^+$	0.32(0.05)	free N_2(5), 36, 59(2), 72, 76(2), 81, 234(2), 237, 251, 255, 268, 289(2), 312, 349(2), 400, 426, 438(2)
free CH_2O		1164, 1247, 1501, 1746, 2766, 2843
$Fe(CH_2O)^+$	0.05(0.01)	free CH_2O, 83, 135, 350
$Fe(CH_2O)_2^+$	0.12(0.02)	free CH_2O(2), 36, 84(2), 153(2), 309, 402, 453(2)
$Fe(CH_2O)_3^+$	0.21(0.04)	free CH_2O(3), 32, 52, 83, 88, 121, 129, 248, 263, 289, 316, 333, 372, 453, 477, 491
$Fe(CH_2O)_4^+$	0.29(0.06)	free CH_2O(4), 35, 49, 60, 96, 100, 124, 143, 204, 246, 266, 269, 282, 337, 348, 354, 369, 377, 443, 455, 506, 534

[a] Uncertainties, listed in parentheses, correspond to ±25% variation in frequencies. [b] B3LYP frequencies for $Fe(CO)_x^+$ are taken from ref 6 and modified as detailed in the text. [c] Based on a T_d symmetry.

At higher energies, some of the cross sections peak and then decline. To model this behavior, we use a modified form of eq 1 that accounts for a decline in the product ion cross section at higher kinetic energies. This model has been described in detail previously[20] and depends on E_D, the energy at which a dissociation channel can begin, and p, a parameter similar to n in eq 1.

Another consideration in the analysis of CID thresholds is the lifetime of the energized complex before dissociation. The lifetime effect is examined by incorporating RRKM theory into eq 1 as previously detailed.[13] The additional information necessary to implement this theory is the set of vibrational frequencies for the transition state (TS) associated with the dissociation. This choice is reasonably straightforward because the TS should be fairly loose and similar to the CID products. This set of vibrational frequencies for the TS is derived from the vibrational frequencies listed in Table 1 by removing one of the metal−ligand stretching frequencies that becomes the dissociation coordinate and reducing the frequencies corresponding to the hindered rotations of the ligand being lost from the cluster. We have arbitrarily reduced the frequencies for the hindered rotations by a factor of 2. This is comparable to the treatment given to $Cr(CO)_x^+$ ($x = 5$, 6)[13] and $M(H_2O)_x^+$ ($x = 4$).[15]

Before comparison with experimental data, the model of eq 1 is convoluted with the kinetic energy distributions of the reactants, as described previously.[10] The parameters σ_0, n, and E_0 are then optimized with a nonlinear least-squares analysis to give the best fit to the data. The optimized value of E_0 is taken to be the measured threshold for a given data set. An estimate of the error in the threshold energy is obtained for variations in E_0 for different data sets, variations in the parameter n, variations in the vibrational frequencies, and the error in the absolute energy scale. Uncertainties listed with the RRKM values also include errors associated with variation in the time assumed available for dissociation (10^{-4} s) by factors of 2 and 1/2.

The cross sections for reaction 2 were modeled using three different strategies.

$$Fe(L)_x^+ + Xe \rightarrow Fe(L)_{x-1}^+ + L + Xe \quad (L = N_2 \text{ or } CH_2O) \qquad (2)$$

First, we modeled the low-energy threshold region where the cross section rises with increasing energy. Second, the cross sections for reaction 2 were modeled over an extended energy range using the modified form of eq 1 that incorporates the parameters p and E_D, as described above. Third, the *total* cross section for $Fe(L)_x^+$ ($x = 2-5$) dissociation was modeled to higher energies, thereby eliminating the need to account for subsequent dissociation. Methods 2 and 3 yield similar E_0 values, which are slightly smaller (by 0.03−0.05 eV) than the values obtained in the first method. The latter two methods represent the cross sections over larger energy ranges than the first, while maintaining good fits in the threshold region. Thus, the values reported in Table 1 are an average of fits obtained using strategies 2 and 3 above.

Vibrational Frequencies. The vibrational frequency for the Fe^+-N_2 stretch has been calculated by Schwarz et al.[8] For larger clusters, we modify the $Fe(CO)_x^+$ ($x = 1-5$) frequencies calculated by Bauschlicher et al.[6] as follows. For all clusters, the frequency of free nitrogen[21] is substituted for the CO stretch. The Fe−C bends, rocks, and wags of all clusters are scaled by a factor of 0.75, the ratio of the Fe−N stretch of $Fe(N_2)^+$ to the Fe−C stretch for $FeCO^+$. Previously, we have used a Morse potential to estimate frequencies.[15] This procedure notes that for a Morse potential the frequency is proportional to $(D_e/\mu)^{1/2}$, where D_e and μ are the equilibrium bond energy and reduced mass, respectively. With this approximation, the ratio of the Fe^+-N_2 to Fe^+-CO frequency is $\omega_1/\omega_2 = [(D_e/\mu)_1/(D_e/\mu)_2]^{1/2} \approx 0.75$, in good agreement with the theoretical result. For larger clusters, $Fe^+(N_2)_x$ ($x = 2-5$), this ratio ranges from 0.75 to 0.81, indicating little change in the correction.

The vibrational frequencies for Fe^+-CH_2O have been calculated[22] and the vibrational frequencies of the larger clusters are estimated from the frequencies for free CH_2O[23] and $Fe(H_2O)_x^+$.[5] The Fe−OCH_2 bends, rocks, and wags and the Fe−O stretching frequencies are taken from the calculated frequencies for similar motions of $Fe(H_2O)_x^+$ clusters scaled by a factor based on a Morse potential, as described above. For clusters of $x = 1-4$, these factors are 0.87, 0.83, 0.92, and 1.00, respectively. The scaling factor for $x = 1$ gives metal−ligand vibrational frequencies of 271, 302, and 452 cm^{-1}, somewhat higher than the calculated values listed in Table 1. The errors introduced by such approximations are very small, however, as can be seen by calculating the average vibrational energies at 298 K for both sets of frequencies. This is 0.03 eV for the frequencies based on scaling the $Fe(H_2O)^+$ frequencies and 0.05 eV (Table 1) for the calculated frequencies. To help estimate such errors in both the N_2 and CH_2O systems, all of the vibrational frequencies used, except the frequencies of free nitrogen and formaldehyde, were scaled by ±25%. The corresponding change in the *average* vibrational energy is taken to be an estimate of one standard deviation of the uncertainty in vibrational energy. This uncertainty is included in the uncertainties in our determination of E_0.

Results

In the following sections, we describe our experimental results for the collision-induced dissociation of the $Fe(N_2)_x^+$ ($x = 1-5$) and $Fe(CH_2O)_x^+$ ($x = 1-4$) clusters. Despite a careful search, we were unable to generate any $Fe(N_2)_x^+$ clusters larger than $x = 5$ and $Fe(CH_2O)_x^+$ clusters larger than $x = 4$.

CID of $Fe(N_2)_x^+$. Results for the interaction of $Fe(N_2)^+$ with Xe are shown in Figure 1. The two products observed correspond to reactions 3 and 4, CID and ligand exchange, respectively.

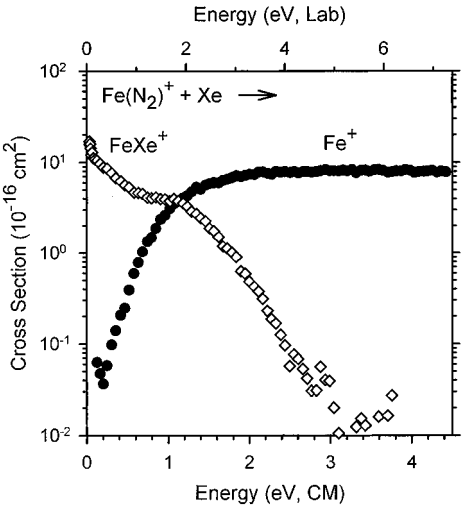

Figure 1. Cross sections for reaction of $Fe(N_2)^+$ with Xe as a function of relative kinetic energy (lower x axis) and laboratory energy (upper x axis).

$$Fe(N_2)^+ + Xe \rightarrow Fe^+ + N_2 + Xe \quad (3)$$

$$\rightarrow FeXe^+ + N_2 \quad (4)$$

The major product at low energies is ligand exchange to form $FeXe^+$. This cross section declines in magnitude until ~1 eV, where it begins to drop more rapidly. At this energy, the complex has enough energy to lose the Xe, and we observe competition with the formation of Fe^+. An analysis of the $FeXe^+$ cross section can be obtained by a detailed comparison to the Langevin−Gioumousis−Stevenson (LGS) model for ion−molecule collisions.[24,25] The observed $FeXe^+$ cross section follows the predicted $E^{-1/2}$ energy dependence from 0.1 to 1.0 eV, but the magnitude is only about 10% of this prediction. The energy dependence differs from σ_{LGS} at lowest energies, <0.1 eV, consistent with a slightly *endothermic* process. Above ~1 eV, the major product is CID to form Fe^+. The Fe^+ cross section rises from an apparent threshold near 0.2 eV and reaches a maximum cross section of about 8 Å^2 around 2 eV.

Cross sections for CID of $Fe(N_2)_2^+$ with Xe are shown in Figure 2. CID to lose one N_2 molecule rises from a threshold of about 0.5 eV to a peak cross section of about 20 Å^2 above 2 eV. Loss of two dinitrogen molecules is a much less probable process, rising from an apparent threshold less than 2 eV to a peak cross section of about 1 Å^2 at 4 eV. The $FeXe^+$ cross section rises from an apparent threshold near 1 eV and rises to a maximum cross section magnitude of 0.5 Å^2 around 2 eV. The cross section then declines at an energy where the $FeXe^+$ molecule can dissociate to $Fe^+ + Xe$.

Cross sections for the CID of $Fe(N_2)_3^+$ and $Fe(N_2)_4^+$ are shown in Figures 3 and 4. They display similar behavior for the primary CID channel with apparent thresholds near zero and peaks of ~50 Å^2 at around 0.8 eV. For $Fe(N_2)_3^+$, loss of a second N_2 is more efficient than for $Fe(N_2)_2^+$, with a peak cross section about 20% of the primary CID channel. At higher energies, formation of $FeXe^+$ rises from a threshold of ~1.5 eV to a peak cross section of ~0.25 Å^2 at 3.0 eV. The cross section declines upon formation of Fe^+, which has an apparent threshold near 2.5 eV and rises to a maximum cross section of 0.6 Å^2.

For $Fe(N_2)_4^+$, the secondary CID channel to form $Fe(N_2)_2^+$ begins at fairly low energies and rises to a maximum cross section of about 30 Å^2. It is the most efficient process at highest energies. The decline in the cross section for $Fe(N_2)_3^+$ above

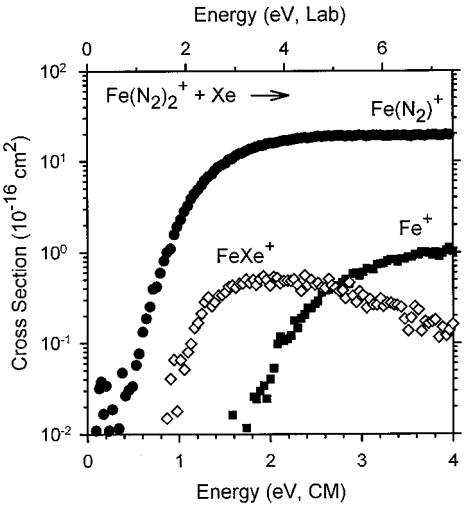

Figure 2. Cross sections for reaction of $Fe(N_2)_2^+$ with Xe as a function of relative kinetic energy (lower *x* axis) and laboratory energy (upper *x* axis).

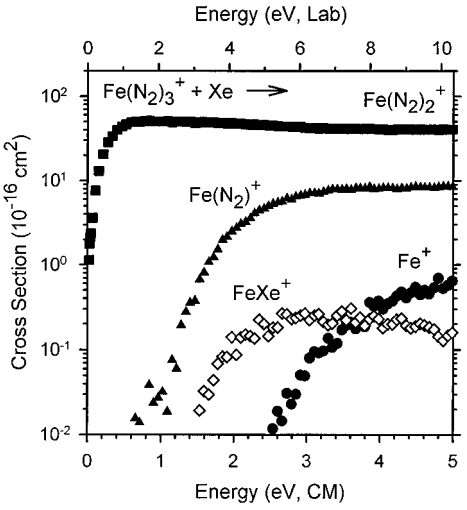

Figure 3. Cross sections for CID of $Fe(N_2)_3^+$ with Xe as a function of relative kinetic energy (lower *x* axis) and laboratory energy (upper *x* axis).

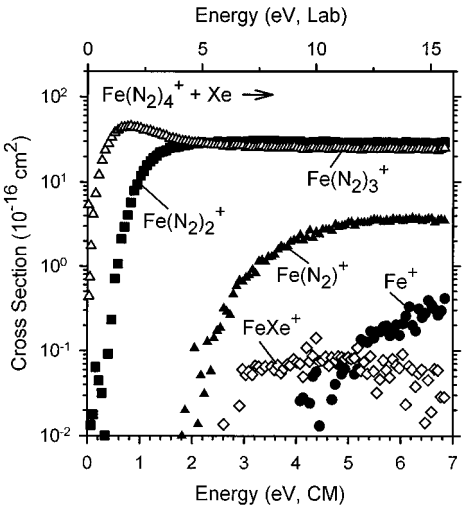

Figure 4. Cross sections for CID of $Fe(N_2)_4^+$ with Xe as a function of relative kinetic energy (lower *x* axis) and laboratory energy (upper *x* axis).

0.6 eV clearly shows that this product dissociates to form the $Fe(N_2)_2^+$ product. The $Fe(N_2)^+$ product channel rises from an apparent threshold around 2 eV to a maximum cross section

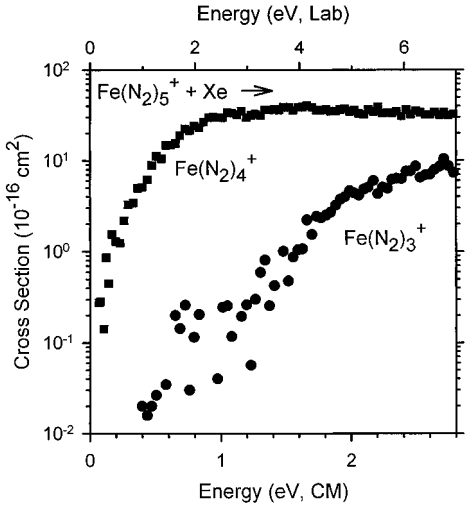

Figure 5. Cross sections for CID of $Fe(N_2)_5^+$ with Xe as a function of relative kinetic energy (lower *x* axis) and laboratory energy (upper *x* axis).

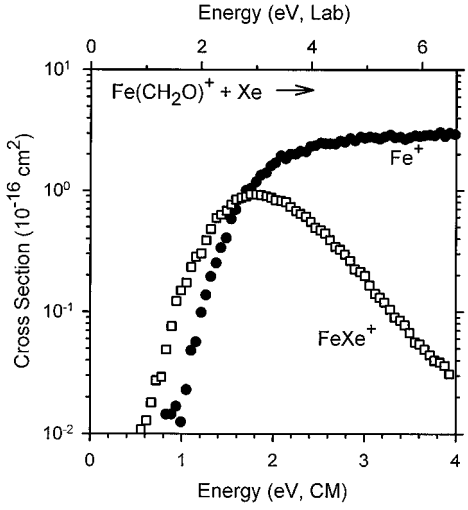

Figure 6. Cross sections for CID of $Fe(CH_2O)^+$ with Xe as a function of relative kinetic energy (lower *x* axis) and laboratory energy (upper *x* axis).

less than 4 Å^2. Less than 1 eV higher in energy, we observe the formation of $FeXe^+$. This peaks at about 0.08 Å^2 at 4 eV and declines upon formation of Fe^+. The Fe^+ cross section rises from an apparent threshold near 4 eV to reach a maximum cross section of 0.4 Å^2.

For the reaction of $Fe(N_2)_5^+$ with Xe, we observe only two product cross sections corresponding to loss of one and two ligands. The cross section to form $Fe(N_2)_4^+$ rises from a threshold near zero to a maximum cross section of about 40 Å^2. About 1 eV higher in energy, we observe loss of a second ligand with a cross section that rises to a maximum of 9 Å^2. Products resulting from further dissociation are not observed because the intensity of the $Fe(N_2)_5^+$ ion beam was too small to provide adequate sensitivity.

For both the N_2 and CH_2O systems, we were unable to detect $Fe(L)_xXe^+$ ($x = 1-5$) clusters because the mass range available to us experimentally limits us to detecting masses below ~220 amu.

CID of $Fe(CH_2O)_x^+$. Results for the interaction of $Fe(CH_2O)^+$ with Xe are shown in Figure 6. The major product at low energies is ligand exchange to form $FeXe^+$. This cross section rises from an apparent threshold below 1 eV to a peak cross section of about 0.9 Å^2 at 1.8 eV. At higher energies,

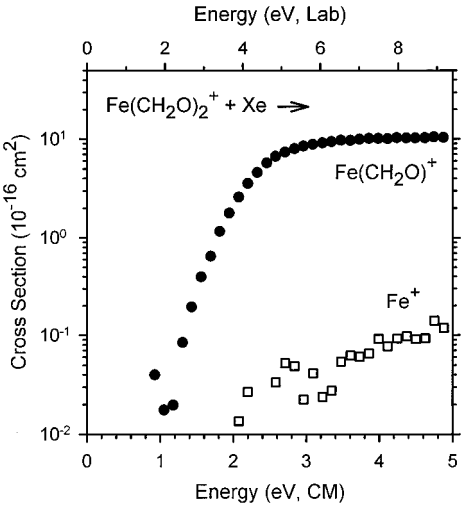

Figure 7. Cross sections for CID of $Fe(CH_2O)_2^+$ with Xe as a function of relative kinetic energy (lower *x* axis) and laboratory energy (upper *x* axis).

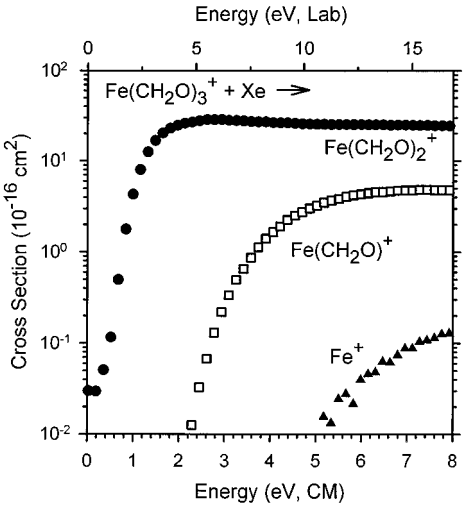

Figure 8. Cross sections for CID of $Fe(CH_2O)_3^+$ with Xe as a function of relative kinetic energy (lower *x* axis) and laboratory energy (upper *x* axis).

the Fe^+ CID product channel rises from an apparent threshold of 1 eV to a maximum cross section of 3 Å^2 at the highest energies.

Cross sections for CID of $Fe(CH_2O)_2^+$ are shown in Figure 7. Primary CID to lose one CH_2O molecule rises from a threshold near 1 eV to a cross section peak of 10 Å^2 at 5 eV. Loss of two formaldehyde ligands is a much less probable process, rising from an apparent threshold above 2 eV to a peak cross section of about 0.1 Å^2 at 5 eV.

Cross sections for the CID of $Fe(CH_2O)_3^+$ and $Fe(CH_2O)_4^+$ are shown in Figures 8 and 9. Loss of one ligand yields the largest product channel in both cases. These reactions have apparent thresholds near zero and magnitudes of ~30 Å^2 at high energies. For $Fe(CH_2O)_3^+$, loss of a second CH_2O ligand has a peak cross section about 20% of the primary CID channel. Losing all three ligands is an extremely inefficient process that occurs above 5 eV to reach a maximum cross section less than 0.2 Å^2.

For $Fe(CH_2O)_4^+$, loss of a second ligand begins at fairly low energies and rises to a maximum cross section of about 15 Å^2. The decline in the cross section for $Fe(CH_2O)_3^+$ above 2 eV clearly shows that this product dissociates to form the $Fe(CH_2O)_2^+$ product. Loss of a third ligand to form $Fe(CH_2O)^+$ rises from an apparent threshold around 3 eV to a maximum cross section of ~1.5 Å^2. Products resulting from further dissociation are not observed because of the small beam size.

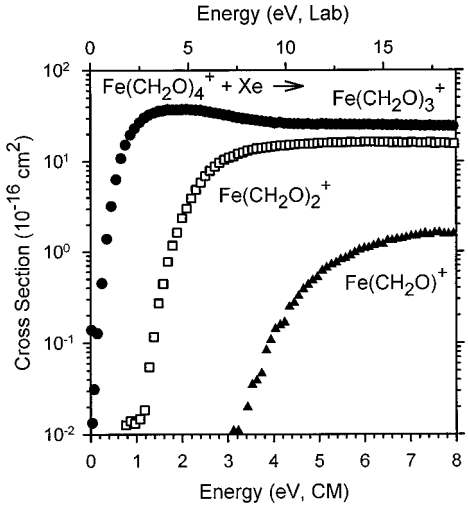

Figure 9. Cross sections for CID of $Fe(CH_2O)_4^+$ with Xe as a function of relative kinetic energy (lower *x* axis) and laboratory energy (upper *x* axis).

TABLE 2: Optimized Fitting Parameters of Eq 1

bond	E_0,[a] eV	σ_0	*n*
Fe^+-N_2	0.56 ± 0.06	8.7 ± 2.7	1.6 ± 0.2
$(N_2)Fe^+-N_2$	0.86 ± 0.09	25.3 ± 3.1	1.8 ± 0.2
$(N_2)_2Fe^+-N_2$	0.47 ± 0.03	55.7 ± 8.2	0.8 ± 0.1
$(N_2)_3Fe^+-N_2$	0.59 ± 0.06	52.0 ± 3.9	1.1 ± 0.1
	0.56 ± 0.04[b]	50.7 ± 3.6	1.1 ± 0.1
$(N_2)_4Fe^+-N_2$	0.70 ± 0.11	74.5 ± 7.4	1.5 ± 0.2
	0.64 ± 0.04[b]	69.9 ± 9.9	1.5 ± 0.2
Fe^+-CH_2O	1.43 ± 0.08	5.5 ± 0.4	1.1 ± 0.2
$(CH_2O)Fe^+-CH_2O$	1.79 ± 0.08	15.0 ± 2.0	1.8 ± 0.2
$(CH_2O)_2Fe^+-CH_2O$	1.08 ± 0.05	41.3 ± 3.7	1.6 ± 0.1
	1.06 ± 0.05[b]	42.9 ± 4.4	1.6 ± 0.1
$(CH_2O)_3Fe^+-CH_2O$	0.88 ± 0.06	61.0 ± 3.2	1.0 ± 0.1
	0.83 ± 0.06[b]	60.9 ± 3.4	1.0 ± 0.1

[a] Equivalent to $D_0(L_{x-1}Fe^+-L)$ at 0 K. [b] Values obtained when including the RRKM analysis; see text.

Thermochemistry. *$(L)_xFe^+-L$ BDEs from Primary Thresholds.* Our best measure of the bond dissociation energies (BDEs) for the iron nitrogen and iron formaldehyde ions comes from measuring the thresholds of the primary dissociation channels, reactions 2. Because the vibrational, rotational, and translational energy distributions of the reactants are explicitly included in our modeling, these thresholds correspond to 0 K values. The 0 K BDEs thus determined are summarized in Table 2 along with the fitting parameters σ_0 and *n* of eq 1. We take the 0 K threshold to equal $D_0[(L)_{x-1}Fe^+-L]$, implicitly assuming that there are no activation barriers to dissociation in excess of the endothermicity. This is generally true for ion−molecule reactions[26,27] and should be valid for the simple bond fission reactions studied here.[28]

In the cases of $Fe(N_2)_x^+$ ($x = 4, 5$) and $Fe(CH_2O)_x^+$ ($x = 3, 4$) two analyses are listed in Table 2: one including the RRKM analysis of the lifetime of the dissociating ion and one ignoring this effect. As the data in Table 2 show, this lifetime effect is substantial for the dissociation of $Fe(N_2)_5^+$ and $Fe(CH_2O)_4^+$ and is considerably smaller for $Fe(N_2)_4^+$ and $Fe(CH_2O)_3^+$. We calculate that the dissociation of $Fe(N_2)_3^+$ and $Fe(CH_2O)_2^+$ is sufficiently prompt that a negligible kinetic shift results. Lifetime effects for the smaller clusters should also be negligible. It is necessary to consider whether the BDEs obtained with or without lifetime considerations are more accurate. Our prejudice is to include the lifetime effect because this consideration has

TABLE 3: $Fe(CO)_x^+$ Bond Dissociation Energies (in eV) at 0 K

species	this study[a]	previous CID[b]	theory[c]
Fe^+-CO ($^4\Sigma^- \rightarrow {}^4F$)[d]	1.59 ± 0.08	1.59 ± 0.08	1.60
Fe^+-CO ($^4\Sigma^- \rightarrow {}^6D$)[e]	1.34 ± 0.04[f]		
$(CO)Fe^+-CO$	1.53 ± 0.05	1.56 ± 0.05	1.60
$(CO)_2Fe^+-CO$	0.73 ± 0.06	0.69 ± 0.06	0.78
	0.71 ± 0.06[g]		
$(CO)_3Fe^+-CO$	1.08 ± 0.06	1.07 ± 0.06	0.98
	1.01 ± 0.06[g]		
$(CO)_4Fe^+-CO$	1.08 ± 0.06	1.16 ± 0.04	0.83
	1.00 ± 0.04[g]		

[a] Reanalysis of data in ref 3. [b] Values originally reported in ref 3. [c] Reference 6, B3LYP values. [d] Diabatic dissociation of $Fe(CO)^+(^4\Sigma^-)$ to $Fe^+(^4F) + CO$. [e] Adiabatic dissociation of $Fe(CO)^+(^4\Sigma^-)$ to ground state $Fe^+(^6D) + CO$. [f] References 40 and 41. [g] Values obtained when including the RRKM analysis; see text.

proved to be critical in the accurate evaluation of the BDEs for transition metal cluster ions,[29] $Cr(CO)_x^+$ ($x = 1-6$) clusters,[13] and alkali metal ion ether complexes.[30]

$FeXe^+$. Analysis of the threshold for the ligand exchange reaction 4 yields a threshold of 0.09 ± 0.06 eV. Because this energy is the difference between the binding energies of N_2 and Xe to Fe^+, $D_0(Fe^+-Xe)$ is determined as 0.47 ± 0.08 eV given the Fe^+-N_2 bond energy of 0.56 ± 0.06 eV (Table 2). This value is within experimental error of a previously derived BDE for Fe^+-Xe of 0.39 ± 0.09 eV, which was determined from ligand exchange reactions of Xe with $Fe(CO)^+$ [3] and $Fe(H_2O)^+$.[2] Our measurement of consistent Fe^+-Xe BDEs from $Fe(CO)^+$, $Fe(H_2O)^+$, $Fe(N_2)^+$, and $Fe(CH_2O)^+$ implies that our source is producing thermalized ions and that it is unlikely that there are any serious systematic errors affecting our threshold determinations in these systems. Alternatively, we can determine an Fe^+-N_2 BDE from the relationship $D_0(Fe^+-N_2) = D_0(Fe^+-Xe) + 0.09 \pm 0.06$ eV. Using our previously determined $D_0(Fe^+-Xe) = 0.39 \pm 0.09$ eV,[42] this yields $D_0(Fe^+-N_2) = 0.48 \pm 0.11$ eV, in good agreement with the directly measured CID value of 0.56 ± 0.06 eV.

An independent measure of the $FeXe^+$ threshold is not made in the formaldehyde system because the $Fe(CH_2O)^+$ beam intensity was generally too small to obtain reliable energy thresholds. In one case (shown in Figure 6) where the signal to noise allows for a good threshold analysis, the measured threshold in the $Fe(CH_2O)^+$ system is consistent with the Fe^+-Xe BDE determined previously.

Fe^+-CO BDEs. In our laboratory's previous assessment of the $(CO)_{x-1}Fe^+-CO$ ($x = 1-5$) BDEs,[3] several assumptions were made concerning the internal energy of the reactant clusters. The vibrational frequencies chosen for $Fe(CO)_5^+$ were taken from the known frequencies for $Fe(CO)_5$ neutral.[31] Several model sets of vibrational frequencies were tested for $Fe(CO)_4^+$ using the neutral $Fe(CO)_5$ frequencies to estimate the corresponding vibrational frequencies for the $Fe(CO)_4^+$ cluster ion. For the $Fe(CO)_x^+$ ($x = 2$, 3) ions, the vibrational frequencies were estimated on the basis of the calculated frequencies of $M(CO)_2^+$, with M = Sc, Cr, and Cu.[32] Lifetime effects of the dissociating ion were not accounted for in the previous analysis by Schultz et al.,[3] as simple calculations indicated they would be negligible.

Recently, vibrational frequencies for $Fe(CO)_x^+$ ($x = 1-5$) have been calculated,[6] and we can now more accurately account for the internal energy of the clusters and determine the kinetic shifts involved with the larger clusters. A reanalysis of the data of Schultz et al.[3] yields the BDEs reported in Table 3, where values with and without lifetime effects are reported for $Fe(CO)_x^+$ ($x = 3-5$). Inspection of these data shows that the values determined without lifetime effects are essentially the same as those reported previously, with the biggest difference being a decrease in the $Fe(CO)_5^+$ threshold. With lifetime effects included in the modeling, we find a small kinetic shift of about 0.08 eV for $Fe(CO)_5^+$ and 0.07 eV for $Fe(CO)_4^+$, and negligible shifts for $Fe(CO)_x^+$ ($x = 1-3$). In concert with several other recent studies of transition metal ion carbonyl bond energies,[13,33-36] we assume that the values obtained with the lifetime effects included are our best values.

Comparison of our new values with the theoretical values obtained by Ricca and Bauschlicher is also done in Table 3.[6] We choose to compare our BDEs to the unaltered B3LYP calculated values because of the arbitrary nature of the adjustments made to "correct" these numbers. It can be seen that the bond energies measured here are close to the theoretical values in all cases but $(CO)_4Fe^+-CO$. The average deviation for the $x = 1-4$ BDEs is 0.04 eV, within our experimental error. Our previous thermochemistry[3] indicated that the fifth carbonyl bond was stronger than the fourth, while the present analysis indicates that these two ligands are bound to Fe^+ nearly equally. This result is in closer agreement with the theoretical result that the fifth bond is somewhat weaker than the fourth.

We can also assess this revised thermochemistry by comparing the sums of the five BDEs, i.e., the heat of reaction for process 5.

$$Fe(CO)_5^+ \rightarrow Fe^+(^6D) + 5CO \qquad (5)$$

Our new values yield a sum of the $(CO)_xFe^+-CO$ bond strengths dissociating to $Fe^+(^6D)$ of 5.61 ± 0.11 eV, given a $Fe^+(^6D) \rightarrow Fe^+(^4F)$ excitation energy of 0.23 eV.[37] This agrees well with the value of 5.58 eV determined by Ricca and Bauschlicher,[5] but is somewhat below the value of 5.92 ± 0.08 eV determined from literature heats of formation of the species in reaction 5, as discussed by Schultz et al.[3] The origin of this discrepancy is not evident. Most of the thermodynamic information used to calculate the literature value for heat of reaction 5 should be very accurate; however, the heat of formation of $Fe(CO)_5$(l) is difficult to measure accurately because complete characterization of the iron oxide products resulting from combustion is difficult (as discussed in the JANAF Tables).[38] This heat of formation has been measured at least twice[39,40] with results that differ by 0.23 eV.[3] Thus, the present results may indicate that an experimental reassessment of this value is in order.

Two additional values for this bond energy sum come from photoionization experiments as the difference in appearance energies for Fe^+ and $Fe(CO)_5^+$. Distefano determined this as 6.05 ± 0.10 eV,[41] and Norwood et al.[42] found 6.50 ± 0.07 eV. As discussed in some detail previously,[3] direct comparison of these values to the present and literature thermochemistry is difficult because it is unclear whether the measured thresholds for Fe^+ correspond to formation of the ^4F excited or ^6D ground state of Fe^+. Further, kinetic shifts associated with losing all five CO ligands from ionized $Fe(CO)_5$ are not assessed. Finally, the thermal energy available in the $Fe(CO)_5$ starting material may need to be accounted for in these experiments. The first two errors serve to shift the sum of bond energies to higher values in the photoionization experiments, while the latter error would decrease the observed sum from its thermodynamic value.

In their paper, Ricca and Bauschlicher[6] contend that the best experimental values available are those of Norwood et al. except that their third bond energy (1.11 ± 0.06 eV) is "overestimated". This suggestion fails to realize that in the photoionization experiments the sequential bond energies are coupled to one another because they represent the differences between the

energy onsets for different products. Thus, shifting the third bond energy down requires that other bond energies be shifted to higher energies. Here, we note that the third bond energy measured in the present experiments (0.71 ± 0.06 eV), by Distefano (0.81 ± 0.10 eV), and directly calculated by Ricca and Bauschlicher (0.78 eV) are consistent.

The Fe^+-CO BDE measured in the CID reaction with Xe yields the diabatic BDE, where $Fe(CO)^+(^4\Sigma^-)$ dissociates to form $Fe^+(^4F) + CO$. The adiabatic process (dissociation to form $Fe^+(^6D) + CO$) is observed in the reactions of $Fe(CO)^+$ with He, D_2, and CH_4.[43,44] The average of these direct measurements of the adiabatic BDE is also included in Table 3. The adiabatic and diabatic values should differ by the $^6D \rightarrow {}^4F$ excitation energy of 0.23 eV.[37] The difference of 0.25 ± 0.09 eV is certainly consistent with this.

Comparison with Literature Thermochemistry. Our value for $D_0(Fe^+-N_2)$, 0.56 ± 0.06 eV, can be combined with additional studies in our laboratory that examine the CID of $Fe(N_2)^+$ with collision gases of Ar, Kr, and CO_2. All experiments yield similar threshold energies, with an average for the four determinations of 0.54 ± 0.05 eV. This value is in excellent agreement with the theoretically determined value of 0.52 ± 0.10 eV.[8] Accompanying this theoretical study was an experimental study involving ligand exchange reactions and equilibrium measurements to bracket the Fe^+-N_2 BDE. An upper limit to the Fe^+-N_2 BDE was established by equilibrium measurements of the relative BDEs of Fe^+-N_2 and Fe^+-Xe. Rate constants for the forward and reverse reactions, $Fe(N_2)^+ + Xe \leftrightarrows FeXe^+ + N_2$, were determined independently and converted into an equilibrium constant at 298 K and $\Delta_rG_{298} = -0.014 \pm 0.004$ eV. From these measurements, an estimate of the $T\Delta_rS$ term = 0.094 ± 0.04 eV, and $\Delta_rH_{298} - \Delta_rH_0 = 0.007 \pm 0.02$ eV, it was determined that N_2 is bound more strongly to Fe^+ than Xe by 0.073 ± 0.065 eV at 0 K. This is in good agreement with the 0.09 ± 0.06 eV difference directly determined in the present study. The observation of ligand exchange reactions at thermal energies of $Fe(N_2)^+$ with C_2H_6, CH_4, and Xe, and the failure to observe ligand displacement with Ar and Kr, was used by Schwarz et al.[8] to determine relative BDEs. Using the lower limit of the calculated Fe^+-Kr BDE as an anchor point yielded $D_0(Fe^+-N_2) > 0.45$ eV, in agreement with the theoretical calculation[8] and the present experimental value.

Cook's kinetic method has been applied by Schwarz et al.[9] to determine the Fe^+-CH_2O BDE. The relative binding energies of various ligands to Fe^+ were evaluated, and using $D_0(Fe^+-C_2H_4) = 1.50 \pm 0.06$ eV[45] as an anchor point, an approximate $D_0(Fe^+-CH_2O) = 1.45 \pm 0.01$ eV was determined.[9] The reported error of 0.01 eV corresponds only to the error associated with the determination of the relative BDE in applying Cook's kinetic method. The absolute error is at least equivalent to the error associated with the anchor point (0.06 eV) and should be larger given uncertainties in estimating the temperature used to describe the internal energy distribution in applying Cook's kinetic method. Our value of 1.43 ± 0.08 eV is in excellent agreement with this number. To our knowledge, none of the larger clusters of $Fe(N_2)_x^+$ or $Fe(CH_2O)_x^+$ have been investigated experimentally or theoretically.

Trends in Sequential Bond Energies. The nonmonotonic variation in the BDEs of iron dinitrogen and iron formaldehyde cluster cations with increasing ligation cannot be rationalized on the basis of increasing steric effects or decreasing effective charge at the metal center. Instead, we turn to a consideration of the electronic structure of these species in order to explain the trends in the sequential bond energies. In our studies of the CID of $M(CO)_x^+$ ions[3,13,33−36] and $M(H_2O)_x^+$ ions,[15] we have explained similar nonmonotonic variations in the sequential BDEs in terms of changes in spin (or lack thereof) of the metal ligand fragments that accompany the removal of ligand molecules. These discussions are reviewed elsewhere.[46] Although electronic state information is not directly provided by these studies, clues to such information are provided by examination of the sequential BDEs.

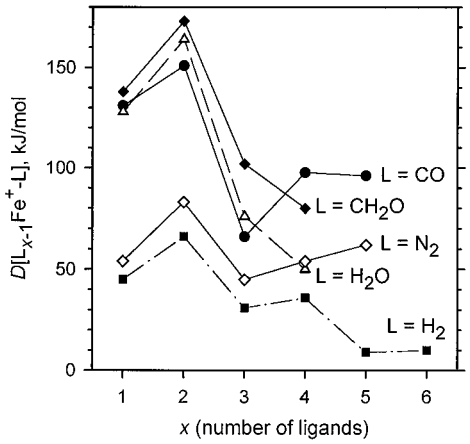

Figure 10. Bond dissociation energies in kJ/mol of iron cation complexes of formaldehyde (diamonds), water (open triangles),[2] carbonyl (circles), dinitrogen (open diamonds), and dihydrogen (squares).[4]

Trends in Fe^+-CH_2O BDEs. For formaldehyde, the strongest bond of the series is $Fe(CH_2O)_2^+$, and the larger cluster BDEs decrease in energy, closely following the trend for the $Fe(H_2O)_x^+$ system, Figure 10. The iron formaldehyde BDEs are stronger than the corresponding Fe^+-H_2O interactions, which presumably reflects the larger dipole moment (2.31 D) and polarizability (2.81 Å^3) of CH_2O compared with H_2O (1.84 D and 1.45 Å^3).[47]

Although the structure of the iron formaldehyde complex has not been determined, it seems likely that the formaldehyde is attached to the metal center through the oxygen atom, a structure similar to $Fe(H_2O)^+$. This aligns the dipole of formaldehyde in the electrostatically favorable orientation and allows the two lone pairs of electrons on oxygen to interact with the metal center to form strong bonds. This structure is supported by the fact that the bonding trends for formaldehyde and water are similar.

The molecular orbitals of H_2O and CH_2O are quite similar.[48] For water, the nonbonding $3a_1$ and $1b_1$ orbitals on oxygen are the σ-donating and π-donating orbitals, respectively. For formaldehyde, the σ-donating orbital is the $5a_1$ orbital, which is largely nonbonding but also has some C−O bond character. Because donating electron density from this orbital will weaken the C−O interaction somewhat, formaldehyde may be a weaker σ-donor than water. The π-donating orbitals are the $1b_2$ (π_{CO}) and $2b_1$ (nonbonding) molecular orbitals of formaldehyde, which lie 1.7 eV below and 1.9 eV above, respectively, the energy level for the π-donating orbital on H_2O.[49] Because the energy levels of the π-donating orbitals are comparable between the water and formaldehyde ligands, formaldehyde should be the stronger π-donor because it can donate π-electron density to the metal center in two planes with the $1b_2$ and $2b_1$ orbitals. Compared to CO, the π-accepting orbital of formaldehyde, the $2b_2$ (π^*_{CO}), is higher in energy by 3.3 eV and should therefore be a weaker π-acceptor.

Ground state $Fe(H_2O)^+$ is calculated to be a $^6A_1$ with bonding derived from the $^6D(3d^64s^1)$ occupation of Fe^+.[5] Theory predicts that the 4s orbital mixes in some 4p character to polarize the 4s electron away from the water ligand, thereby reducing the Fe^+-water repulsion. A $^4A_1$ state of $Fe(H_2O)^+$ is calculated

to lie about 0.04 eV higher in energy than the sextet state[5] and correlates with the $^4F(3d^7)$ state of atomic Fe^+. Here, the repulsion from the 4s electron is removed, and the repulsion in the σ space is further reduced by 4s−3dσ hybridization. The energy necessary to promote the 4s electron from the ^6D state to achieve the ^4F configuration (0.23 eV)[37] is slightly larger than the reduced repulsion associated with removal of the 4s electron and the 4s−3dσ hybridization.[5]

The similarities of H_2O and CH_2O suggest that the $Fe(CH_2O)^+$ complex should form strong bonds with either the $^6D(4s^13d^6)$ or $^4F(3d^7)$ configurations of Fe^+. Formaldehyde (with a slightly larger dipole moment than water) should be capable of polarizing the electron in the 4s orbital away, as in the $Fe(H_2O)^+$ ($^6A_1$) complex. However, unpublished theoretical studies[22] suggest that the ground state of $Fe(CH_2O)^+$ is a quartet that lies ∼0.61 eV lower in energy than the sextet,[22] although the quartet−sextet energy splitting is probably overestimated. The level of theory used for this calculation predicts that the $^4F(3d^7)$ excited state of Fe^+ is 0.1 eV more stable than the $^6D(4s^13d^6)$ ground state, while experimentally, the ^6D state is found to be 0.23 eV lower in energy than the $^4F(3d^7)$ state.[37] Correcting for this error in the asymptotic energies places the quartet state of $Fe(CH_2O)^+$ ∼0.18 eV lower than the sextet state. Because calculations on both species indicate that the quartet and sextet states for $Fe(H_2O)^+$ and $Fe(CH_2O)^+$ are close in energy, additional theoretical work should include calculations on both species at the same level of theory in order to definitively determine their respective ground states.

Calculations for the larger $Fe(CH_2O)_x^+$ ($x = 2-4$) clusters have not been performed, but we can imagine the bonding in the larger clusters will be similar to $Fe(H_2O)_x^+$ ($x = 2-4$). With two H_2O molecules sharing the cost of promotion and 4s−3dσ hybridization, the $Fe(H_2O)_2^+$ has a quartet ground state with linear O−Fe^+−O geometry.[5] This change in bonding results in a binding energy for the second water that is larger than that of the first water by approximately the promotion energy of 0.23 eV. The 4s−3dσ hybridization moves the electron density to an orbital perpendicular to the metal−ligand axis.[5] Consequently, the second ligand can see a higher nuclear charge if it approaches from the side opposite the first ligand.

The third and fourth water BDEs are weaker than the first two. Theory finds that both $Fe(H_2O)_x^+$ ($x = 3, 4$) complexes have quartet ground states.[5] The calculated $Fe(H_2O)_3^+$ structure is very different from other $Fe(L)_3^+$ systems, such as $Fe(CO)_3^+$, where the 4s−3dσ hybridization is lost and the ligands are arranged in a manner that minimizes the ligand−ligand repulsion (planar geometry with an L−M−L angle of ∼120°). The structure for $Fe(H_2O)_3^+$ starts from a planar arrangement but one of the L−M−L angles is ∼80° and the third ligand axis bisects this angle. This allows 4s−3dσ hybridization to be partially maintained, although efficiency of 4s−3dσ hybridization to reduce metal−ligand repulsion is much less than for $Fe(H_2O)_2^+$, thereby weakening the third H_2O ligand BDE.[5] The optimal structure for $Fe(H_2O)_4^+$ is between a square planar and tetrahedral structure and can be thought of by starting with a square planar structure, distorting toward tetrahedral, and then moving opposite pairs of water ligands closer together (L−M−L angle of ∼80°). This structure again allows some 4s−3dσ hybridization to be retained, but seems to be a compromise between ligand−ligand repulsion and metal in-plane and metal out-of-plane lone-pair repulsion.[5]

The first and second bond energies for the formaldehyde system are about 0.1 eV stronger than in the water system, and the third and fourth bond energies are about 0.3 eV stronger in the formaldehyde system. As noted above, some of this increase can be attributed to the larger polarizability and dipole moment of CH_2O. The larger increase in bond energy for the larger clusters may be because of decreased ligand−ligand repulsion in the formaldehyde system. This may simply be because the hydrogen atoms in $Fe(CH_2O)_x^+$ complexes are further removed from the metal center and thus from each other, given similar FeL_x^+ geometries for both the formaldehyde and water systems. This rationale seems reasonable if the structures for $Fe(H_2O)_3^+$ and $Fe(H_2O)_4^+$, and likewise $Fe(CH_2O)_3^+$ and $Fe(CH_2O)_4^+$, are strongly influenced by ligand−ligand repulsion as suggested by theory.[5] Alternatively, the stronger binding in $Fe(CH_2O)_x^+$ complexes could be explained by formaldehyde being a stronger π-donating ligand than water. If this is the case, the larger $Fe(CH_2O)_x^+$ complexes probably have more symmetric geometries than the water complexes.

Trends in $Fe(N_2)_x^+$ BDEs. As shown in Figure 10, the trends in BDEs for the $Fe(CO)_x^+$ and $Fe(N_2)_x^+$ series are similar, which can be rationalized on the basis of the formally isoelectronic character of the CO and N_2 ligands. Empirically, we find that the BDE of $Fe(L)_2^+$ is the strongest bond of each series and the third ligand binds most weakly. N_2, a weaker ligand in both its π-accepting and σ-donating abilities, has bond strengths averaging only 57 ± 10% of the carbonyl species.

Both $Fe(CO)^+$ and $Fe(N_2)^+$ are calculated to have $^4\Sigma^-$ ground states with an Fe^+ occupation of $3d\sigma^13d\pi^43d\delta^2$.[6,8] This occupation minimizes the Fe^+−ligand repulsion in the σ orbitals and maximizes the metal to ligand π back-donation. The repulsion in the σ space is further reduced by 4s−3dσ hybridization. Calculations for the larger nitrogen clusters have not been performed, but we can imagine that the bonding is similar to the analogous carbonyl species.[6] Thus, the bonding in $Fe(N_2)_2^+$ should be similar to that in $Fe(N_2)^+$, with the second N_2 on the opposite side of the metal as the first ligand. This enables both ligands to benefit from the 4s−3dσ hybridization, which reduces the electron density on both sides of the Fe^+. The second N_2 is more strongly bound than the first, as the cost of the 4s−3dσ hybridization and promotion from $4s^13d^6$-(^6D) to $3d^7(^4F)$ state of Fe^+ has been paid by the first ligand.

When the third ligand is added, there is a significant drop in the binding energy. For the $Fe(CO)_3^+$ and $Fe(H_2)_3^+$ complexes, this has been attributed to the loss of 4s−3dσ hybridization[3,4] and thus seems likely in the N_2 series as well. For the N_2 series, the bond energy increases slightly upon addition of a fourth N_2 ligand, behavior similar to that in the $Fe(CO)_x^+$ and $Fe(H_2)_x^+$ systems but in sharp contrast with the $Fe(H_2O)_x^+$ and $Fe(CH_2O)_x^+$ systems. It has been rationalized[5,50] that an increase from the third to the fourth ligand BDE can result if there is similar bonding in the two species, but the energy lost upon disruption of 4s−3dσ hybridization is paid by the third ligand.

The fourth and fifth CO ligands are bound equally, while the fifth N_2 ligand is bound slightly more strongly than the fourth, results that are inconsistent with increased ligand−ligand repulsion. Theory[6] has calculated a quartet ground state for $Fe(CO)_3^+$, a doublet for $Fe(CO)_5^+$, and that $Fe(CO)_4^+$ has doublet and quartet states that are too close in energy to definitively determine the ground state. Nevertheless, a spin change must occur somewhere between the third and fifth ligands. Comparison of the BDE trends for $Fe(H_2)_x^+$ ($x = 1-6$),[4] which are all calculated to have quartet ground states,[7] helps elucidate where the spin change probably occurs in the N_2 series. As shown in Figure 10, the $Fe(H_2)_x^+$ ($x = 1-4$) BDEs parallel the $Fe(N_2)_x^+$ series; however, the fifth H_2 ligand is weakened significantly compared to the fourth, whereas the Fe^+-N_2 BDEs continue to increase from 3 to 5. Because we observe an *increase* in the bond strength of the fifth N_2 ligand,

this suggests that a quartet−doublet spin change occurs in the N_2 ligand system. The pattern of bond energies can be rationalized if the $Fe(N_2)_5^+$ complex has a doublet ground state and the $Fe(N_2)_4^+$ complex has either a doublet ground state or a quartet ground state with a low-lying doublet excited state.

This hypothesis seems reasonable in terms of traditional ligand field theory. In coordinatively saturated complexes, the assignment of high-spin vs low-spin states depends on whether the splitting in the metal orbitals is larger than the electron-pairing energy. Strong field ligands induce larger splittings and therefore tend to form low-spin complexes. In odd-electron systems, the splitting of the d orbitals increases as additional ligands are added until a low-spin doublet state is the preferred ground state. Apparently four or five N_2 or CO ligands are required to reach this point, while H_2, a weaker field ligand, is unable to do this with six ligands.

Differences in $Fe(L)_4^+$. An obvious difference between the trends in bond energies for the π-donating systems (H_2O, CH_2O) and the π-accepting systems (CO, N_2, H_2) is the strength of the fourth ligand. For the π-donating ligands, this bond energy continues to decrease from the third ligand, whereas for the π-accepting ligands, this bond energy actually increases compared to the third ligand, Figure 10. Examination of the orbital energy level diagrams for the two "textbook" geometries of a four-coordinate system, square planar and tetrahedral, may provide some understanding of this fundamental difference.

In a square planar geometry (with the *z* axis as the symmetry axis), the *xz*, *yz*, and *xy* (π-like) orbitals are lowest in energy with the z^2 orbital somewhat higher. The x^2-y^2 orbital, which points at the ligands, is very high in energy. Therefore for Fe^+ in a doublet state, the seven electrons would have a $(xz)^2(yz)^2(xy)^2(z^2)^1$ configuration. To achieve a quartet state, an electron would have to be promoted to the high-lying x^2-y^2 orbital. Because the doubly occupied *xy*, *xz*, and *yz* orbitals in the square planar geometry are available for π back-donation, this configuration strongly favors π-accepting ligands. For a tetrahedral geometry, the degenerate z^2 and x^2-y^2 orbitals are low in energy and the degenerate *xy*, *xz*, and *yz* orbitals lie higher in energy. A quartet Fe^+ would have a $(z^2)^2(x^2-y^2)^2(xy)^1(xz)^1(yz)^1$ configuration, where the singly occupied orbitals can act as π-acceptors. A doublet state (which would undergo a Jahn−Teller distortion) must lie higher in energy for this geometry. Therefore, this geometry favors π-donating ligands.

These qualitative ideas make the prediction that four π-accepting ligands should be able to form low-lying low-spin doublet states having square planar geometries. Binding in such states should be favorable because electrons are removed from orbitals pointed at the ligands and placed in orbitals that can be used for π back-donation. High-spin quartet states having tetrahedral geometries may also be low in energy for π-accepting ligands. In contrast, π-donating ligands have no energetically favorable means of accessing a geometry that allows a doublet state. Therefore, these simple ideas predict that π-donating ligands should have quartet ground states and that doublet states should be fairly high in energy.

These simple considerations can now be checked by comparison with high-level ab initio calculations on $Fe(CO)_4^+$, $Fe(H_2)_4^+$, and $Fe(H_2O)_4^+$. The quartet and doublet state of $Fe(CO)_4^+$ have been determined[6] to have a tetrahedral and a square planar structure, respectively, closely following the qualitative ideas outlined above. Theoretical information on $Fe(H_2)_4^+$ and $Fe(H_2O)_4^+$ shows that their structures are more complex. Theory[4] finds that the structure of $Fe(H_2)_4^+$ is neither square planar nor tetrahedral. Rather, the fourth ligand binds out of plane at approximately right angles to the first three ligands, which are basically planar (in essence, an octahedral field with the two open positions cis to one another). Bushnell, Kemper, and Bowers[4] speculate that this geometry is favored over a square planar because of the involvement of the valence 4p orbitals on the metal. Another possible consideration notes that the octahedral-like field allows the z^2 and x^2-y^2 orbitals to have similar energies, which would be favorable for a quartet state. Because H_2 is a much weaker field ligand than CO, a low-spin doublet state is energetically unfavorable (even after six H_2 ligands have been added), but the π-accepting ability of the H_2 ligand heavily favors geometries that allow π back-donation. Because the square planar geometry discriminates so heavily against quartet states, the $Fe(H_2)_4^+$ complex maintains the octahedral-like character that allows good π back-donation but allows the energy of the x^2-y^2 orbital to decrease significantly. As discussed above, the structure of $Fe(H_2O)_4^+$ is somewhere in between a square planar and tetrahedral geometry.[5] One interesting way of viewing this distortion starts by noting that the calculated[5] electron configuration is $(z^2)^2(xy)^2(xz)^1(yz)^1(x^2-y^2)^1$. This orbital energy ordering can be obtained from the square planar configuration, $xy < xz = yz < z^2 < x^2-y^2$, noted above by destabilizing the π-like orbitals (*xy*, *xz*, and *yz*) until they lie above the z^2, which is lowered in energy by $4s-3d\sigma$ hybridization. Distortion toward the tetrahedron allows the energy of the x^2-y^2 orbital to decrease in order to allow the quartet spin state. It is no surprise that the detailed calculations provide geometries for the FeL_4^+ complexes that are more complicated than the simple ligand field ideas allow; nevertheless, these ideas do permit a simple characterization of the empirically observed difference in the bond energies for π-donating and π-accepting ligands. To be useful, the more detailed theories need to better elucidate why these classes of ligands exhibit such qualitatively different behavior.

Acknowledgment. This work is supported by the National Science Foundation, Grant No. CHE-9530412.

References and Notes

(1) Hinton, J. F. *Solvent Effects on Chemical Phenomena*; Academic Press: New York, 1973; Vol. 1. Dogonadze, R. R.; Kálmán, E.; Koryshev, A. A.; Ulstrup, J. *The Chemical Physics of Solvation*, 3 vols; Elsevier: Amsterdam, 1985; *Faraday Discuss. Chem. Soc.* **1988**, *85*.

(2) Schultz, R. H.; Armentrout, P. B. *J. Phys. Chem.* **1993**, *97*, 596.

(3) Schultz, R. H.; Crellin, K. C. Armentrout, P. B. *J. Am. Chem. Soc.* **1991**, *113*, 8590.

(4) Bushnell, J. E.; Kemper, P. R.; Bowers, M. T. *J. Phys. Chem.* **1995**, *99*, 15602.

(5) Ricca, A.; Bauschlicher, C. W., Jr. *J. Phys. Chem.* **1995**, *99*, 9003.

(6) Ricca, A.; Bauschlicher, C. W., Jr. *J. Phys. Chem.* **1994**, *98*, 12899.

(7) Maitre, P.; Bauschlicher, C. W., Jr. Manuscript in preparation, as cited in ref 4.

(8) Schwarz, J.; Heinemann, C.; Schwarz, H. *J. Phys. Chem.* **1995**, *99*, 11405.

(9) Schröder, D.; Schwarz, H. *J. Organomet. Chem.* **1995**, *504*, 123.

(10) Ervin, K. M.; Armentrout, P. B. *J. Chem. Phys.* **1985**, *83*, 166.

(11) Schultz, R. H.; Armentrout, P. B. *Int. J. Mass Spec. Ion Processes* **1991**, *107*, 29.

(12) Teloy, E.; Gerlich, D. *Chem. Phys.* **1974**, *4*, 417. Gerlich, D. Diplomarbeit, University of Freiburg, Federal Republic of Germany, 1971.

(13) Khan, F. A.; Clemmer, D. E.; Schultz, R. H.; Armentrout, P. B. *J. Chem. Phys.* **1993**, *97*, 7978.

(14) Dalleska, N. F.; Honma, K.; Armentrout, P. B. *J. Am. Chem. Soc.* **1993**, *115*, 12125.

(15) Dalleska, N. F.; Honma, K.; Sunderlin, L. S.; Armentrout, P. B. *J. Am. Chem. Soc.* **1994**, *116*, 3519.

(16) Loh, S. K.; Lian, L.; Hales, D. A.; Armentrout, P. B. *J. Chem. Phys.* **1988**, *89*, 3378.

(17) Hales, D. A.; Lian L.; Armentrout, P. B. *Int. J. Mass Spectrom. Ion Processes* **1990**, *102*, 269.

(18) Aristov, N.; Armentrout, P. B. *J. Am. Chem. Soc.* **1986**, *108*, 1806, and references therein.

(19) Beyer, T.; Swinehart, D. F. *Commun. ACM* **1973**, *16*, 379. Stein, S. E.; Rabinovitch, B. S. *J. Chem. Phys.* **1973**, *58*, 2438; *Chem. Phys. Lett.*

1977, *49*, 183. Gilbert, R. G.; Smith, S. C. *Theory of Unimolecular and Recombination Reactions*; Blackwell Sci.: Oxford, 1990.

(20) Weber, M. E.; Elkind, J. L.; Armentrout, P. B. *J. Chem. Phys.* **1986**, *84*, 1521.

(21) Huber, K. P.; Herzberg, G. *Molecular Spectra and Molecular Structure IV*; Van Nostrand Reinhold Co.: New York, 1979; p 420.

(22) Schröder, D. Personal communication.

(23) Shimanouchi, T. *Tables of Molecular Vibrational Frequencies*; U. S. Government Printing Office: Washington, DC, 1972; Consolidated Vol. I, NSRDS-NBS 39.

(24) Gioumousis, G.; Stevenson, D. P. *J. Chem. Phys.* **1958**, *29*, 292.

(25) The LGS model for the collision cross section of an ion−molecule reaction at low energies is given by $\sigma_{LGS} = \pi e(2\alpha/E)^{1/2}$, where e is the electron charge, α is the polarizability of the target molecule (4.02 Å^3 for Xe), and E is the relative kinetic energy of the reactants.

(26) Armentrout, P. B. In *Advances in Gas Phase Ion Chemistry*; Adams, N. G., Babcock, L. M., Eds.; JAI: Greenwich, 1992; Vol. 1, pp 83−119.

(27) Boo, B. H.; Armentrout, P. B. *J. Am. Chem. Soc.* **1987**, *109*, 3459. Ervin, K. M.; Armentrout, P. B. *J. Chem. Phys.* **1987**, *86*, 2659. Elkind, J. L.; Armentrout, P. B. *J. Phys. Chem.* **1984**, *88*, 5454. Armentrout, P. B. In *Structure/Reactivity and Thermochemistry of Ions*; Ausloos, P., Lias, S. G., Eds.; Reidel: Dordrecht, 1987; pp 97−164.

(28) Armentrout, P. B.; Simons, J. *J. Am. Chem. Soc.* **1992**, *114*, 8627.

(29) Armentrout, P. B.; Hales, D. A.; Lian, L. In *Advances in Metal and Semiconductor Clusters*; Duncan, M. A., Ed.; JAI: Greenwich, 1994; Vol 2; pp 1−39.

(30) More, M. B.; Glendening, E. D.; Ray, D.; Feller, D.; Armentrout, P. B. *J. Phys. Chem.* **1996**, *100*, 1605.

(31) Jones, L. H.; McDowell, R. S.; Goldblatt, M.; Swanson, B. I. *J. Chem. Phys.* **1972**, *57*, 2050.

(32) Barnes, L. A.; Rosi, M.; Bauschlicher, C. W., Jr. *J. Chem. Phys.* **1990**, *93*, 609.

(33) Goebel, S.; Haynes, C. L.; Khan, F. A.; Armentrout, P. B. *J. Am. Chem. Soc.* **1995**, *117*, 6994.

(34) Khan, F. A.; Steele, D. A.; Armentrout, P. B. *J. Phys. Chem.* **1995**, *99*, 7819.

(35) Meyer, F.; Chen, Y.-M.; Armentrout, P. B. *J. Phys. Chem.* **1995**, *117*, 4071.

(36) Sievers, M.; Armentrout, P. B. *J. Phys. Chem.* **1995**, *99*, 8135.

(37) j-level averaged value from: Moore, C. E. *Atomic Energy Levels*; National Standard Reference Data Series; National Bureau of Standards, NSRDS-NBS 35: Washington, DC, 1971.

(38) Chase, M. W., Jr.; Davies, C. A.; Downey, J. R., Jr.; Frurip, D. J.; McDonald, R. A.; Syverud, A. N. *J. Phys. Chem. Ref. Data* **1985**, *14*, Suppl. 1.

(39) Mittasch, A. *Angew. Chem.* **1928**, *41*, 827.

(40) Cotton, F. A.; Fischer, A. K.; Wilkinson, G. *J. Am. Chem. Soc.* **1959**, *81*, 800.

(41) Distefano, G. *J. Res. Natl. Bur. Stand., Sect. A* **1970**, *74*, 233.

(42) Norwood, K.; Ali, A.; Flesch, G. D.; Ng, C. Y. *J. Am. Chem. Soc.* **1990**, *112*, 7502.

(43) Tjelta, B. L.; Armentrout, P. B. *J. Am. Chem. Soc.* **1995**, *117*, 5531.

(44) Tjelta, B. L.; Armentrout, P. B. *J. Am. Chem. Soc.* **1996**, *118*, 9652.

(45) Armentrout, P. B.; Kickel, B. L. In *Organometallic Ion Chemistry*; Freiser, B. S., Ed.; Kluwer: Dordrect, 1995; pp 1−45.

(46) Armentrout, P. B. *Acc. Chem. Res.* **1995**, *28*, 430.

(47) Rothe, E. W.; Bernstein, R. B. *J. Chem. Phys.* **1959**, *316*, 1619.

(48) Jorgensen, W. L.; Salem, L. *The Organic Chemist's Book of Orbitals*; Academic Press: New York, 1973.

(49) Kimura, K.; Katsumata, S.; Achiba, Y.; Yamazaki, T.; Iwata, S. *Handbook of HeI Photoelectron Spectra of Fundamental Organic Molecules*; Halstad Press: New York, 1981.

(50) Haynes, C. L.; Armentrout, P. B.; Perry, J. K.; Goddard, W. A., III. *J. Phys. Chem.* **1995**, *99*, 6340.